Anharmonic lattice dynamics and thermal transport of monolayer InSe under equibiaxial tensile strains

Zezhu Zeng[1], Shasha Li[1 2], Terumasa Tadano[3] and Yue Chen[1 4]

[1]Department of Mechanical Engineering, The University of HongKong, HongKong
[2]School of Science, Nanjing University of Posts and Telecommunications, Nanjing 210023, China
[3]Research Center for Magnetic and Spintronic Materials, National Institute for Materials and Science, Tsukuba, Japan
[4]HKU Zhejiang Institute of Research and Innovation, 1623 Dayuan Road, Lin An 311305, China

E-mail: yuechen@hku.hk

Abstract. Two-dimensional (2D) InSe, which exhibits high electron mobility and a wide band gap has emerged as a promising material for photoelectric and thermoelectric applications. The inadequate understanding of the lattice thermal conductivity (κ), however, hampers the advancement of 2D InSe. Herein, by taking into account anharmonicity up to the fourth order and introducing the equibiaxial tensile strain (ϵ), we have performed an in-depth study on the lattice dynamics of 2D InSe. Interestingly, the κ exhibits a non-monotonic behaviour as a function of equibiaxial tensile strain, which can be attributed to the changes in acoustic phonon lifetimes. At the Γ point, a blue-shift of the lowest optical mode and a red-shift of the uppermost optical mode are reported for the first time. More strikingly, the blue-shift can be largely suppressed by equibiaxial tensile strain. Further study indicates that the unique transition of the potential energy surface is responsible for the disappearance of the blue-shift. Our work may enlighten the future research on phonon engineering and management of the lattice thermal conductivity of 2D InSe.

Keywords: monolayer InSe, thermal transport, phonon anhamonic properties, perturbation theory

1. Introduction

Tremendous research on two-dimensional materials in recent years has indicated that their properties have greatly distinct differences from those of the parent materials. Recently, monolayer indium selenide (InSe) has been studied because of its outstanding electronic and optical properties. It is promising for nanoelectronic device applications because of its high carrier mobility. [1] Monolayer InSe also exhibits excellent optical second-order susceptibility, and it can be a candidate for photodetector devices. [2–6] Additionally, due to its high electron mobility and direct semiconducting band gap, it is particularly promising for photovoltaic and solar cell applications. [7–10] The ultralow

thermal conductivity also provides broad prospects in the thermoelectric field. [11–14] Nevertheless, it is still immature for the industrial applications. A critical issue is how to manipulate the thermal conductivity to improve the performance and efficiency of devices. For instance, carrier thermalisation typically occurs in a few picoseconds because of quick thermal transport, which limits the efficiency of solar cells, hence a significant slowing of carrier cooling and the reduction of κ by phonon engineering are required. [15–18] On the other hand, fast and effective heat removal significantly determines the service life of nanoelectronic devices, so in some cases it is necessary to increase κ to extend the device lifetime.

Strain engineering as a powerful method has always been used to modify the thermal properties. [19–22] Recently, a large tunability of the lattice thermal conductivity of monolayer silicene via strain has been reported. [23] Liu et al. found the disparate strain dependent thermal conductivity of 2D penta-structures, [24] and ding et al. also used the strain engineering to extensively control the phonon scattering rates and κ of 2D MoS_2, [20] so it is advisable to apply the strain to adjust the phonon scattering processes and κ. To explore the intrinsic principles of lattice thermal transport, it is important to understand phonons, which are heat excitations in crystals. For instance, Nissimagoudar et al. have studied the lattice thermal conductivity and size effects of 2D InSe and found that the lattice thermal conductivity is much lower than that of graphene and MoS_2. [8] Zhou et al. showed the unique harmonic phonon behaviour and ultralow thermal conductance of monolayer InSe. [25] However, the intrinsic anharmonic phonon scattering mechanisms and strain engineering that can be utilized to regulate the κ have not been systematically studied.

Unlike some of the 2D materials with simple honeycomb structures, such as graphene and h-BN, which are composed of a single atomic layer, 2D InSe is composed of four atomic layers. The top and bottom layers both consist of Se atoms, while the middle two layers consist of In atoms. The crystal structure of monolayer InSe is shown in Fig. 1. The relatively complex buckling structure and multi-layer coupling may induce unique lattice dynamics. In this work, the lattice anharmonicity of monolayer InSe is explored based on first-principles calculations. A non-monotonic relationship between the lattice thermal conductivity and strain is reported. The contributions of different phonon branches to the κ and the variation of phonon lifetime under different equibiaxial tensile strains have been studied to explain the unusual strain dependent behaviour. We use three perturbative self energy diagrams (tadpole, bubble and loop diagrams) to analyse the strain dependent phonon frequency shifts. [26–28] The unique transition of the potential energy surface (PES) with increasing strains is also discussed to rationalize the phonon coupling. The phonon anharmonic properties are expected to pave the way for further thermal optimization and applications of monolayer InSe.

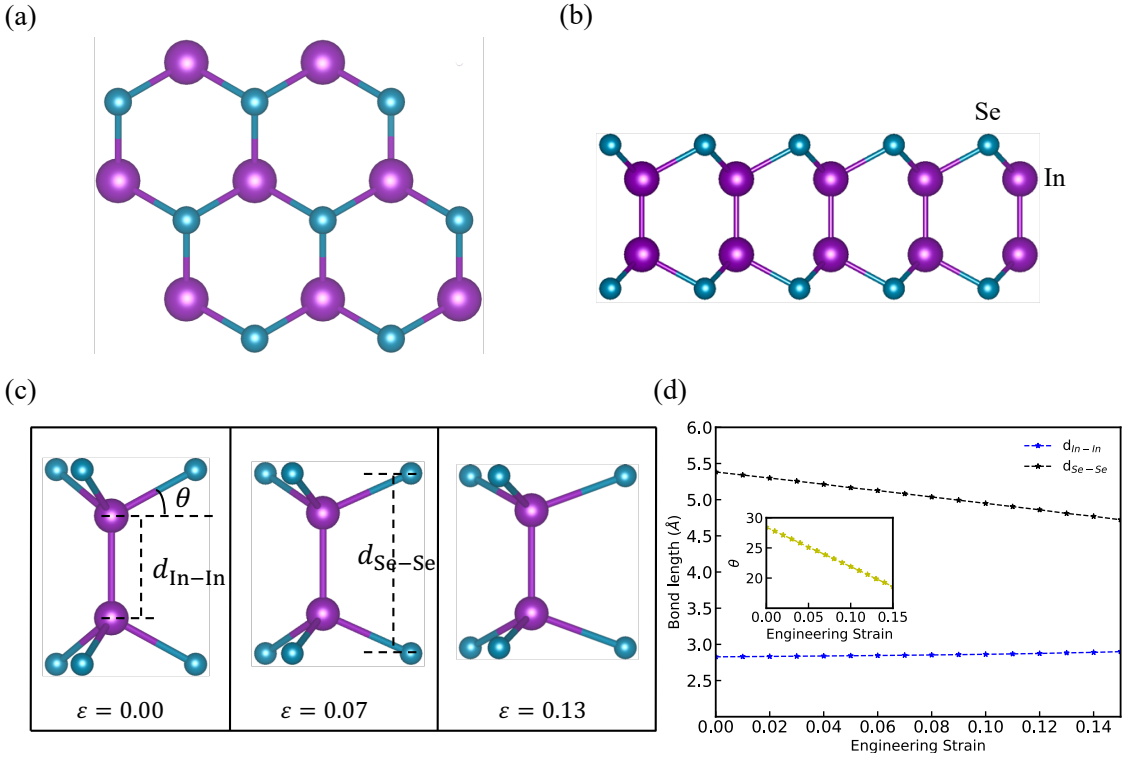

Figure 1. The top view (a) and side view (b) of the crystal structure of 2D InSe. (c) Evolution of the crystal structure under different equibiaxial tensile strains. (d) Evolutions of bond lengths and angle θ as a function of equibiaxial tensile strain.

2. Methodology

Perturbation theory is an effective method to unearth the intrinsic phonon anharmonicity. The anharmonic terms can be expressed as a perturbation H' of the harmonic Hamiltonian H_0 as: [29]

$$H = H_0 + H' \approx H_0 + W_3 + W_4. \tag{1}$$

Here, we only consider the third-order (W_3) and fourth-order (W_4) terms since the contributions of higher-order terms are much smaller. The anharmonic self energy $\mathbf{\Pi}_{\boldsymbol{qj}}(\omega)$ can be extracted by the one-phonon Green's function and Dyson equation. [30] There are three main Feynman diagrams to describe the anharmonic phonon self energy. The bubble and tadpole diagrams are the second-order Feynman diagrams resulting from the cubic term and the loop diagram is the lowest-order Feynman diagram of the quartic term, therefore the loop diagram is generally more critical to phonon frequency shift than the bubble and tadpole diagrams. [31–35]

The phonon frequency shift $\Delta_{\boldsymbol{qj}}$ and half width at half maximum $\Gamma_{\boldsymbol{qj}}$ are given as $\Delta_{\boldsymbol{qj}} = -\frac{1}{\hbar}\mathrm{Re}\Pi_{\boldsymbol{qj}}(\omega_{\boldsymbol{qj}})$ and $\Gamma_{\boldsymbol{qj}} = \frac{1}{\hbar}\mathrm{Im}\Pi_{\boldsymbol{qj}}(\omega_{\boldsymbol{qj}})$. Because the bubble diagram is complex while the tadpole and loop diagrams are real, the total frequency shift and linewidth

are given as follows: [36]

$$\Delta_{\boldsymbol{q}j}^{\mathrm{tot}} = -\frac{1}{\hbar}\left(\Pi_{\boldsymbol{q}j}^{\mathrm{tadpole}} + \Pi_{\boldsymbol{q}j}^{\mathrm{loop}} + \mathrm{Re}\Pi_{\boldsymbol{q}j}^{\mathrm{bubble}}(\omega_{\boldsymbol{q}j})\right), \tag{2}$$

$$\begin{aligned}\Gamma_{\boldsymbol{q}j}^{\mathrm{bubble}}(\omega) = \frac{\pi}{2\hbar^2}\sum_{\boldsymbol{q}_1,\boldsymbol{q}_2}\sum_{j_1,j_2}|V^{(3)}_{-\boldsymbol{q}j,\boldsymbol{q}_1 j_1,\boldsymbol{q}_2 j_2}|^2 \\ \times\left[-(n_1+n_2+1)\delta(\omega+\omega_1+\omega_2)+(n_1+n_2+1)\delta(\omega-\omega_1-\omega_2)\right. \\ \left.-(n_1-n_2)\delta(\omega-\omega_1+\omega_2)+(n_1-n_2)\delta(\omega+\omega_1-\omega_2)\right].\end{aligned}$$

After obtaining the frequency shift and linewidth, the phonon power spectrum $\chi''_{\boldsymbol{q}j}(\Omega)$ is given by the Lorentz function

$$\chi''_{\boldsymbol{q}j} \propto \frac{1}{\pi}\left[\frac{\Gamma_{\boldsymbol{q}j}^{\mathrm{bubble}}(\omega_{\boldsymbol{q}j})}{(\Omega-(\Omega_0+\Delta_{\boldsymbol{q}j}^{\mathrm{tot}}))^2+(\Gamma_{\boldsymbol{q}j}^{\mathrm{bubble}}(\omega_{\boldsymbol{q}j}))^2}\right], \tag{3}$$

where Ω_0 represents the harmonic frequency value. To analyse the origin of phonon frequency shifts, we calculated the potential energy surface (PES) of a phonon mode by displacing the atoms by: [37]

$$\boldsymbol{u}_s = \frac{\eta}{\sqrt{NM_s}}\boldsymbol{e}_\mu(s,\boldsymbol{q}j). \tag{4}$$

Here, N is the number of unit cells in the supercell and M_s is the mass of the s atom. η and $\boldsymbol{e}_\mu(s,\boldsymbol{q}j)$ are the amplitudes of the normal coordinate and the eigenvector, respectively.

First-principles calculations were performed using the Vienna Ab-initio Simulation Package (VASP) [38]. The energy cutoff was fixed to 400 eV. Self-consistent calculations were continued until the total electronic energy difference between two steps became less than 10^{-7} eV. The projector augmented wave (PAW) method and Perdew-Burke and Ernzerhof (PBE) functional were used to calculate the electron-ion [39] and exchange-correlation interactions. [40] A vacuum space of 25 Å was applied along the z direction to exclude interactions between adjacent cells. The harmonic and anharmonic force constants were extracted from ALAMODE. [41] [42] A $6 \times 6 \times 1$ supercell (144 atoms), and a $2 \times 2 \times 1$ Monkhorst Pack grid were used to calculate the second order force constants. A $5 \times 5 \times 1$ supercell (100 atoms) and a $3 \times 3 \times 1$ Monkhorst Pack grid were used to calculate the anharmonic force constants. The force cutoff radius was set to the 11th and 3rd neighbouring atom distances to extract the third- and fourth-order force constants, respectively. Note that the fourth-order force constants were used to calculate the contribution of loop diagram to phonon frequency shift. The relaxation time approximation (RTA) and the tetrahedron method with a q-mesh of $250 \times 250 \times 2$ were used to calculate the lattice thermal conductivity. For low-κ materials, the RTA method can also work well for the calculation of κ because of the dominant Umklapp processes. Nissimagoudar et al. have used both the RTA and iterative methods to calculate the κ of 2D InSe [8] and the results are similar. Compared with the Gaussian

smearing method, the tetrahedron method eliminates the error from the evaluation of the δ function, and allows more accurate calculation of phonon lifetimes. After applying the equibiaxial strain, the internal coordinates of all atoms were fully relaxed. The splitting of the longitudinal optical mode and transverse optical mode (LO-TO splitting) was also taken into account (More information about convergence tests is available in the Supplementary materials).

3. Results and Discussion

Monolayer InSe has a honeycomb structure with a lattice constant of 4.09 Å. The In-In and Se-Se bond lengths of the unstrained structure are 2.83 Å and 5.38 Å, respectively, both of which agree very well with previous DFT calculations. [43] [44] The structures under 0%, 7%, and 13% strains are shown in Fig. 1c. It can be seen that the tensile strain reduces the bond angle and buckling distance. The Se-Se bond length continuously decreases with increasing strains, while the In-In bond length is almost unchanged, as shown in Fig. 1d, which implies that the perpendicular distance between Se atoms and In atoms decreases under larger tensile strain.

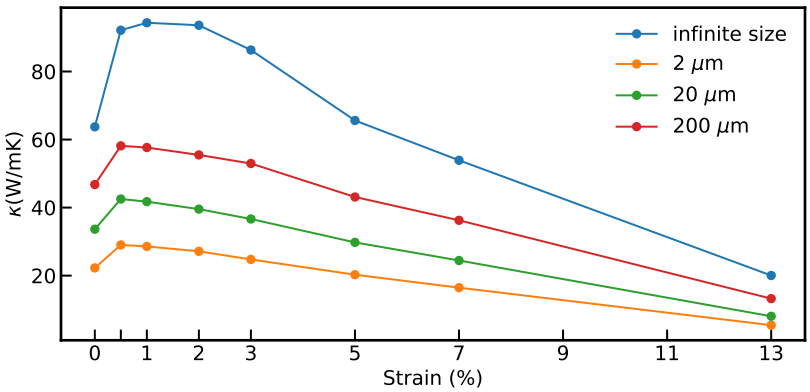

Figure 2. The lattice thermal conductivity of monolayer InSe at infinite and finite sample sizes (2, 20 and 200 μm) at room temperature as a function of equibiaxial strain.

The primitive cell of monolayer InSe has four atoms, thus there are three acoustic phonon branches and nine optical branches. To conveniently describe each branch, they are labelled by a number index according to the frequency values. We used the perpendicular distance between the uppermost Se atom and the bottom Se atom as the thickness (d_{Se-Se}) of monolayer InSe to calculate the lattice thermal conductivity. It should be noted that the lattice thermal conductivity of 2D InSe also diverges with the q-mesh in the infinite size as in the case of silicene, [23] which may result from some acoustic phonon modes that have extremely long phonon wavelengths. More information about the convergence of κ is shown in the Supplementary materials.

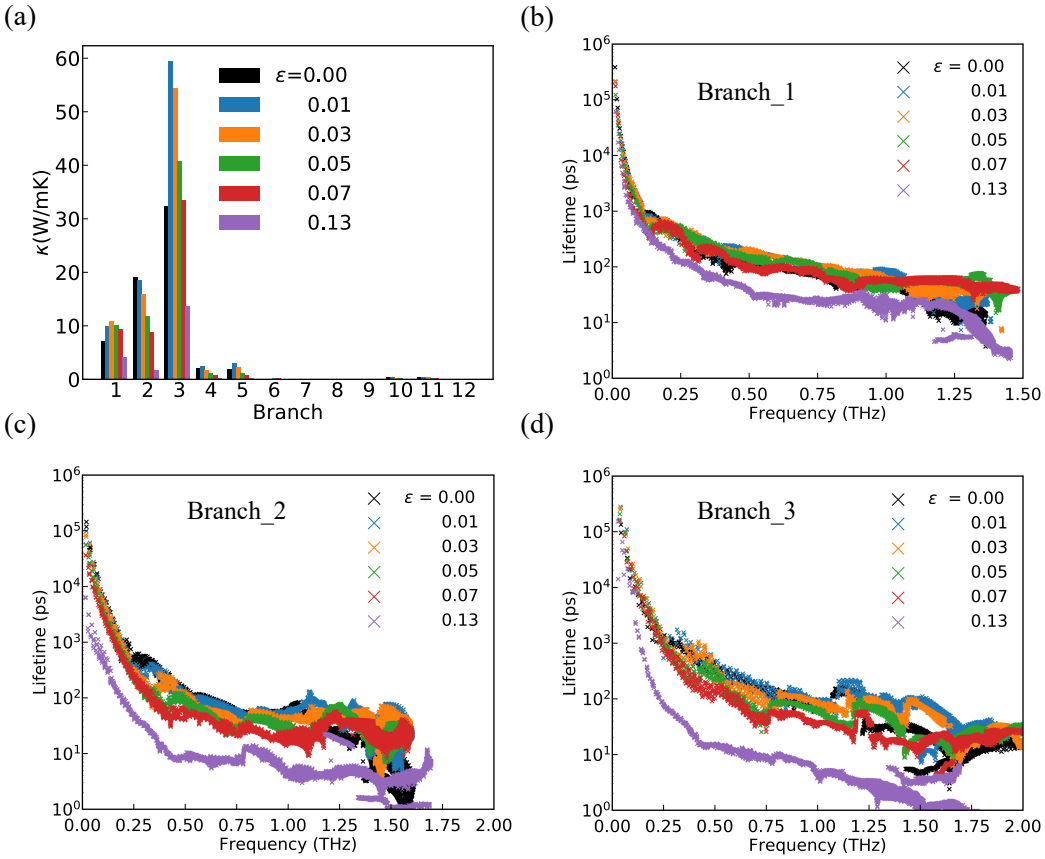

Figure 3. (a) The contributions of different phonon branches to the lattice thermal conductivity of 2D InSe. The phonon lifetimes under different equibiaxial strains as a function of frequency (b-d).

The non-monotonic behavior of the lattice thermal conductivity as a function of equibiaxial tensile strain is shown in Fig. 2. The κ of the unstrained structure at room temperature is 63.73 W/mK. We noticed that our κ value is slightly larger than the previous result, [8] which may result from the difference of the integral method in the Brillouin zone. Under equibiaxial strain, the highest κ value (93.58 W/mK at 300 K) appears at a strain of 1%. When the strain continues to increase, the κ is rapidly suppressed as expected. As the size effect can induce the boundary scattering, which imposes a limit on the phonon mean free path (MFP) and eliminates the divergence of κ at the infinite size, we also consider the sample sizes of 2, 20 and 200 μm. From Fig. 2, it is apparent that the κ of the unstrained structure is enhanced from 22.25 W/mK to 46.74 W/mK with increasing of sample size from 2 μm to 200 μm, which indicates that some phonon modes in monolayer InSe have a long MFP. It is noted that the non-monotonic behaviour of κ exists in all sample size systems even though the highest κ lying at the strain of 0.5 %.

It is unusual that monolayer InSe exhibits a non-monotonic strain dependent lattice thermal conductivity. In fact, for bulk materials, such as diamond [45] and silicon, [46] their lattice thermal conductivities show a conventional monotonic strain

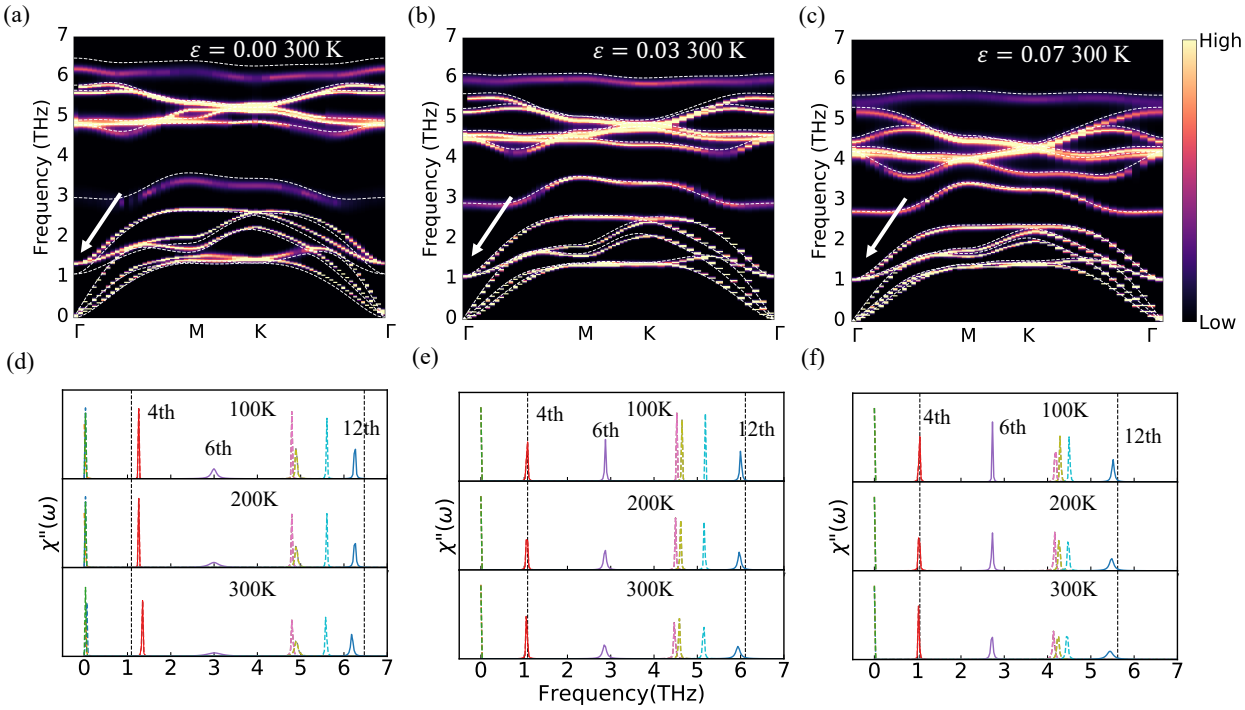

Figure 4. Phonon spectra of 2D InSe under (a) 0.00, (b) 0.03, and (c) 0.07 equibiaxial strains at 300K. The white dashed lines represent the harmonic phonon disersion. The phonon spectra at Γ point under (d) 0.00, (e) 0.03, and (f) 0.07 equibiaxial strains at different temperatures. The vertical black dashed lines represent the corresponding harmonic phonon frequencies. The area under each phonon peak is normalized to one.

dependence. In some 2D materials, such as $PtSe_2$ [47] and MoS_2, [48] their lattice thermal conductivities can be largely suppressed by equibiaxial tensile strain. It was found from empirical molecular dynamics simulations that the thermal conductivities of graphene and MoS_2 [19, 20] also decreases with tensile strain. For some 2D materials that have buckling structures, such as silicene and penta-structure materials [23,24], non-monotonic behaviour of κ under strain is observed and attributed to the transition of the buckling distance in the 2D structures. For instance, the buckling distance in silicene also has a non-monotonic strain dependence, which implies that the thermal conductivity of silicene has a strong correlation with the buckling distance. [23] However, in 2D InSe, we observe a monotonic strain dependent buckling distance even though the lattice thermal conductivity has a non-monotonic strain dependence. Furthermore, Zhu et al. made a comprehensive study of the thermal transport behaviors of 2D boron nitride and the superlattices comprised by 2D boron nitride and graphene under tensile strains, and found that their thermal conductivities also show the nonmonotonic behavior with strain. They attributed this behavior to the competition between in-plane softening and flexural stiffening of acoustic phonons branches [49]

To further comprehend the non-monotonic κ, we first studied the contribution from different phonon branches under equibiaxial strains. In Fig. 3a, it is clear that the higher-frequency branches (from the 4th branch to the 12th branch) only make very

small contributions to the overall κ, so the non-monotonic κ behaviour is mainly due to the contributions of the acoustic branches. From the Boltzmann thermal transport equation, we know that there are three crucial parameters that mainly govern the lattice thermal conductivity: the group velocity, heat capacity, and phonon lifetime. The group velocity and heat capacity have insignificant variations under equibiaxial strains (see Fig. s3 in the Supplementary materials), so phonon lifetime dominates the changes of κ under strains. It is noted that the non-monotonic relationship between κ and strain in silicene is also governed by the large tunability of the phonon lifetime. [23]

Due to the slight contributions of high-frequency phonon branches to the lattice thermal conductivity, we focus on the phonon lifetimes of the three lowest-frequency branches. The relationship between strain and the contribution of the first branch to κ is also found to be non-monotonic. The contribution of the first branch to κ continuously increases for strain from 0% to 3% but decreases from 3% to 13%. The transition of the phonon lifetime with strain in Fig. 3b is consistent with the transition of the contribution to κ; the phonon lifetime also increases with strain from 0% to 3% and decreases with strain from 3% to 13%. A similar non-monotonic behaviour also exists in the third phonon branch, of which the aggregate contribution to the overall lattice thermal conductivity is more than 45% for the unstrained structure. When applying an equibiaxial tensile strain of 1%, there is an almost two times of enhancement to the contribution to κ (from 31.08 W/mK to 59.36 W/mK at 300 K). The apparent fluctuation of the phonon lifetime in the third branch (Fig. 3d) rationalizes the non-monotonic behaviour. On the one hand, the phonon lifetimes in the third branch are generally larger than the first and second branches, which results in a dominant contribution from the third branch to the total κ. On the other hand, the largest phonon lifetimes exist under a strain of 1%, which is consistent with the peak location of the strain dependent κ as shown in Fig. 2. The second phonon branch has the usual transition tendency with the strain. The phonon lifetime of the second branch monotonically decreases with increasing strain. Due to the much smaller contribution to the κ compared with the third branch, 2D InSe still has a non-monotonic lattice thermal conductivity behaviour.

The phonon frequency shifts and linewidths of some specific modes of 2D InSe exhibit an unusual strain dependence. We extracted the third- and fourth-order force constants to calculate the phonon self energies and obtain the phonon frequency shifts. To illustrate the frequency shifts, we first plotted the phonon spectra under different strains at 300 K in Fig. 4. For the unstrained structure, the fourth branch has an obvious blue-shift with an increase of temperature from 0 K (white dashed line) to 300 K, especially at the Γ point (see the white arrow). The twelfth branch has an apparent red-shift throughout the entire Brillouin zone. We also notice that there is a very wide phonon linewidth in the sixth phonon branch. These features of phonon imply strong anharmonicity in unstrained monolayer InSe.

Interestingly, these optical phonon branches have different reactions to equibiaxial tensile strain. The blue-shift completely vanishes at strains of 0.03 and 0.07 as shown in

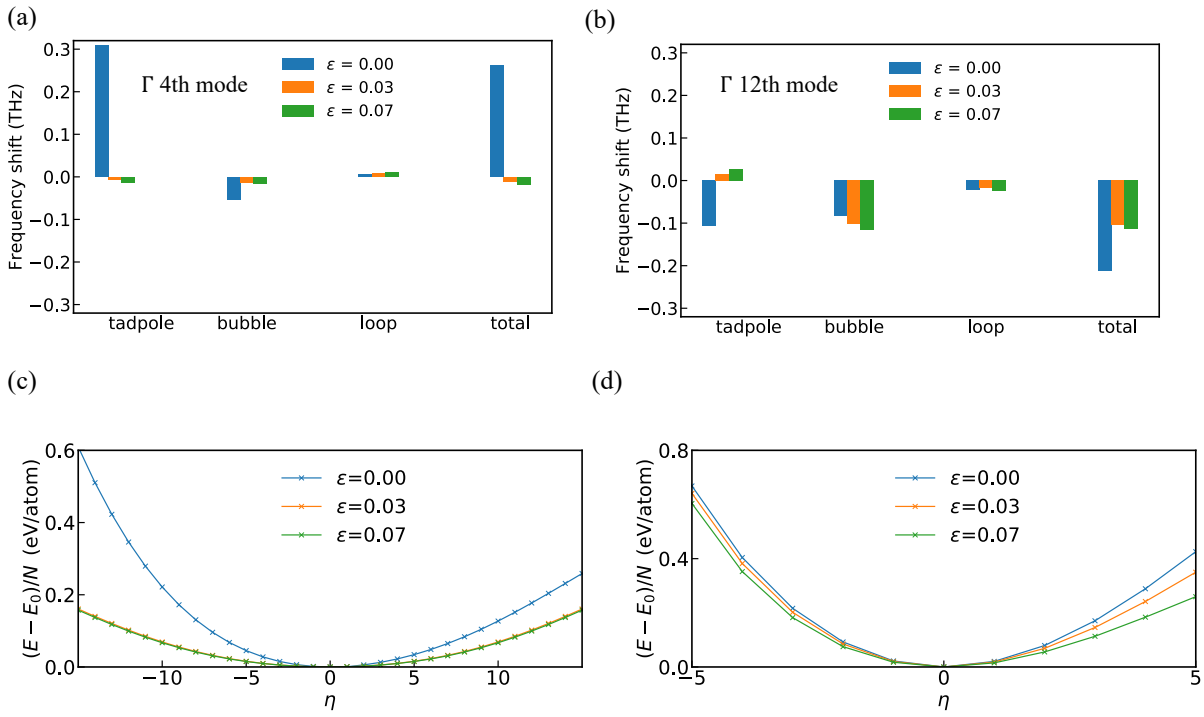

Figure 5. Phonon frequency shifts of the fourth (a) and the twelfth (b) modes at Γ point under different equibiaxial strains at 300 K, and the contributions from the tadpole, bubble and loop terms. The PES corresponding to the fourth (c) and the twelfth (d) phonon modes at Γ point.

Fig. 4b and Fig. 4c, respectively. While the red-shift of the twelfth phonon mode still exists but the amplitude is slightly suppressed under strain. To show these frequency shifts more clearly, the phonon spectra at the Γ point at different temperatures are also shown in Fig. 4. With the increasing temperature, the fourth branch moves towards the high-frequency region, while the twelfth branch moves towards the low-frequency region. After applying equibiaxial strains, the temperature dependent frequency shift of the fourth branch is completely suppressed. Additionally, the amplitude of the red-shift of the twelfth phonon mode decreases under strain. It is also noted that the strain also has a significant effect on the linewidth of the sixth phonon branch. In Fig. 4a and 4d, it is apparent that the sixth phonon branch shows very large linewidths and thus very small phonon lifetimes. The linewidth of the sixth branch significantly decreases under equibiaxial tensile strains (Fig. 4e and 4f); whereas, the linewidth of the twelfth phonon mode increases with increasing strains. The different strain dependence of linewidth of these phonon modes may be attributed to the redistribution of three-phonon phase space or the changes of third-order anharmonic force constants under strain. As these optical phonon modes do not significantly contribute to the lattice thermal conductivity, the changes in their linewidths have a minor effect on the κ of 2D InSe.

To further comprehend the origin of the phonon frequency shifts, we extracted the contributions of the three perturbation terms (tadpole, bubble and loop) corresponding

to the fourth phonon mode at the Γ point at equibiaxial tensile strains of 0.00, 0.03 and 0.07. Fig. 5a shows that the tadpole term makes the most significant contribution to the blue-shift of unstrained 2D InSe. This is unusual, because the first-order perturbation of the fourth-order anharmonic term (loop diagram) usually makes a major contribution to the frequency shift, as shown in previous reports [33, 35, 50, 51]. Moreover, the frequency shift contributed by the tadpole diagram is almost inhibited under equibiaxial tensile strain, which results in a suppression of the blue-shift. For the red-shift of the twelfth phonon mode at the Γ point when $\epsilon = 0.00$, it is also found that the third order perturbation terms (the tadpole and bubble diagrams) make more significant contributions than the fourth order term. After applying equibiaxial strains, the tadpole term is also greatly suppressed, resulting in a reduction of the amplitude of the red-shift.

The tadpole diagram is usually related to the structural symmetry. If the internal atomic coordinates are determined by the crystal symmetry, then the contribution of the tadpole term is zero. [34, 52] However, In and Se atoms in the primitive cell of 2D InSe occupy the 2h ($\frac{1}{3}$,$\frac{2}{3}$,z) and 2i ($\frac{2}{3}$,$\frac{1}{3}$,z) Wyckoff positions, respectively. [53] The z coordinates of In and Se atoms cannot be determined by the symmetry, thus the tadpole term may play a crucial role in the phonon frequency shift of monolayer InSe. Nevertheless, the dominant blue-shift disappears under equibiaxial tensile strains because of the remarkable reduction of the tadpole diagram contribution, as shown in Fig. 5a.

In Fig. 5c, the PES of the fourth phonon mode at the Γ point under different equibiaxial strains is shown. At $\epsilon = 0.00$, the PES is strongly asymmetric, suggesting large contributions from the third-order anharmonic terms, which is consistent with the large blue-shift contributed by the tadpole diagram. When equibiaxial tensile strain is applied, the third-order contributions are reduced and the PES becomes more symmetrical, resulting in a suppression of the blue-shift. Therefore, the correlation between the frequency shift of the fourth phonon mode at the Γ point and strain can be attributed to the unique transition of the PES. In Fig. 5d, the PES corresponding to the twelfth phonon mode at Γ point is also shown. It is seen that equibiaxial tensile strain results in a more asymmetric PES, which may be related to the contributions of the tadpole and bubble terms to phonon frequency shift.

4. Conclusions

By employing the first-principles calculations, we studied the lattice anharmonicity of monolayer InSe under different equibiaxial tensile strains. The non-monotonic lattice thermal conductivity of 2D InSe as a function of strain has been reported. Phonon lifetimes at different strains were calculated to rationalize this unusual behaviour. The third phonon branch plays a critical role in the non-monotonic strain dependence of the lattice thermal conductivity. A blue-shift of the fourth phonon branch and a red-shift of the twelfth phonon branch are also reported for unstrained 2D InSe at elevated temperatures. The blue-shift of the fourth phonon mode at the Γ point is found to

result from the contribution of the tadpole diagram, and to be related to the crystal symmetry and the strongly asymmetric PES. This phonon blue-shift is very sensitive to equibiaxial tensile strains and is suppressed after applying strains of 3% and 7%; the strain dependence is found to be related to the transition of the PES. Our findings provide a more complete understanding of the phonon anharmonicity and its strain dependence in 2D InSe, which may be instructive for thermal transport engineering.

5. Acknowledgements

This work is supported by the National Natural Science Foundation of China (51706192 and 11874313), Environment and Conservation Fund (69/2018), and Zhejiang Provincial Natural Science Foundation (LR19A040001). The authors are grateful for the research computing facilities offered by ITS, HKU.

6. References

[1] Denis A Bandurin, Anastasia V Tyurnina, L Yu Geliang, Artem Mishchenko, Viktor Zólyomi, Sergey V Morozov, Roshan Krishna Kumar, Roman V Gorbachev, Zakhar R Kudrynskyi, Sergio Pezzini, et al. High electron mobility, quantum hall effect and anomalous optical response in atomically thin inse. *Nature Nanotechnology*, 12(3):223, 2017.

[2] Jiadong Zhou, Jia Shi, Qingsheng Zeng, Yu Chen, Lin Niu, Fucai Liu, Ting Yu, Kazu Suenaga, Xinfeng Liu, Junhao Lin, et al. Inse monolayer: synthesis, structure and ultra-high second-harmonic generation. *2D Materials*, 5(2):025019, 2018.

[3] Zhesheng Chen, Johan Biscaras, and Abhay Shukla. A high performance graphene/few-layer inse photo-detector. *Nanoscale*, 7(14):5981–5986, 2015.

[4] Sidong Lei, Fangfang Wen, Liehui Ge, Sina Najmaei, Antony George, Yongji Gong, Weilu Gao, Zehua Jin, Bo Li, Jun Lou, et al. An atomically layered inse avalanche photodetector. *Nano Letters*, 15(5):3048–3055, 2015.

[5] Srinivasa Reddy Tamalampudi, Yi-Ying Lu, Rajesh Kumar U, Raman Sankar, Chun-Da Liao, Karukanara Moorthy B, Che-Hsuan Cheng, Fang Cheng Chou, and Yit-Tsong Chen. High performance and bendable few-layered inse photodetectors with broad spectral response. *Nano Letters*, 14(5):2800–2806, 2014.

[6] David K Sang, Huide Wang, Meng Qiu, Rui Cao, Zhinan Guo, Jinlai Zhao, Yu Li, Quanlan Xiao, Dianyuan Fan, and Han Zhang. Two dimensional β-inse with layer-dependent properties: Band alignment, work function and optical properties. *Nanomaterials*, 9(1):82, 2019.

[7] Sidong Lei, Liehui Ge, Sina Najmaei, Antony George, Rajesh Kappera, Jun Lou, Manish Chhowalla, Hisato Yamaguchi, Gautam Gupta, Robert Vajtai, et al. Evolution of the electronic band structure and efficient photo-detection in atomic layers of inse. *ACS Nano*, 8(2):1263–1272, 2014.

[8] Arun S Nissimagoudar, Jinlong Ma, Yani Chen, and Wu Li. Thermal transport in monolayer inse. *Journal of Physics: Condensed Matter*, 29(33):335702, 2017.

[9] Ching-Hwa Ho and Yun-Ju Chu. Bending photoluminescence and surface photovoltaic effect on multilayer inse 2d microplate crystals. *Advanced Optical Materials*, 3(12):1750–1758, 2015.

[10] J Zhang, XY Lang, YF Zhu, and Q Jiang. Strain tuned inse/mos 2 bilayer van der waals heterostructures for photovoltaics or photocatalysis. *Physical Chemistry Chemical Physics*, 20(26):17574–17582, 2018.

[11] Tribhuwan Pandey, David S Parker, and Lucas Lindsay. Ab initio phonon thermal transport in monolayer inse, gase, gas, and alloys. *Nanotechnology*, 28(45):455706, 2017.

[12] Nguyen T Hung, Ahmad RT Nugraha, and Riichiro Saito. Two-dimensional inse as a potential thermoelectric material. *Applied Physics Letters*, 111(9):092107, 2017.

[13] Guang Han, Zhi-Gang Chen, John Drennan, and Jin Zou. Indium selenides: structural characteristics, synthesis and their thermoelectric performances. *Small*, 10(14):2747–2765, 2014.

[14] Leonard W Sprague Jr, Cancan Huang, Jeong-Pil Song, and Brenda M Rubenstein. Maximizing thermoelectric figures of merit by uniaxially straining indium selenide. *The Journal of Physical Chemistry C*, 2019.

[15] GJ Conibeer, D König, MA Green, and JF Guillemoles. Slowing of carrier cooling in hot carrier solar cells. *Thin Solid Films*, 516(20):6948–6953, 2008.

[16] Ana M Brown, Ravishankar Sundararaman, Prineha Narang, William A Goddard III, and Harry A Atwater. Nonradiative plasmon decay and hot carrier dynamics: effects of phonons, surfaces, and geometry. *Acs Nano*, 10(1):957–966, 2015.

[17] Hiroki Kawai, Giacomo Giorgi, Andrea Marini, and Koichi Yamashita. The mechanism of slow hot-hole cooling in lead-iodide perovskite: first-principles calculation on carrier lifetime from electron–phonon interaction. *Nano Letters*, 15(5):3103–3108, 2015.

[18] Haining Wang, Jared H Strait, Paul A George, Shriram Shivaraman, Virgil B Shields, Mvs Chandrashekhar, Jeonghyun Hwang, Farhan Rana, Michael G Spencer, Carlos S Ruiz-Vargas, et al. Ultrafast relaxation dynamics of hot optical phonons in graphene. *Applied Physics Letters*, 96(8):081917, 2010.

[19] Xiaobo Li, Kurt Maute, Martin L Dunn, and Ronggui Yang. Strain effects on the thermal conductivity of nanostructures. *Physical Review B*, 81(24):245318, 2010.

[20] Zhiwei Ding, Qing-Xiang Pei, Jin-Wu Jiang, and Yong-Wei Zhang. Manipulating the thermal conductivity of monolayer mos2 via lattice defect and strain engineering. *The Journal of Physical Chemistry C*, 119(28):16358–16365, 2015.

[21] Kathryn F Murphy, Brian Piccione, Mehdi B Zanjani, Jennifer R Lukes, and Daniel S Gianola. Strain-and defect-mediated thermal conductivity in silicon nanowires. *Nano Letters*, 14(7):3785–3792, 2014.

[22] Youdi Kuang, Lucas Lindsay, and Baoling Huang. Unusual enhancement in intrinsic thermal conductivity of multilayer graphene by tensile strains. *Nano Letters*, 15(9):6121–6127, 2015.

[23] Han Xie, Tao Ouyang, Éric Germaneau, Guangzhao Qin, Ming Hu, and Hua Bao. Large tunability of lattice thermal conductivity of monolayer silicene via mechanical strain. *Physical Review B*, 93(7):075404, 2016.

[24] Huake Liu, Guangzhao Qin, Yuan Lin, and Ming Hu. Disparate strain dependent thermal conductivity of two-dimensional penta-structures. *Nano Letters*, 16(6):3831–3842, 2016.

[25] Hangbo Zhou, Yongqing Cai, Gang Zhang, and Yong-Wei Zhang. Unusual phonon behavior and ultra-low thermal conductance of monolayer inse. *Nanoscale*, 10(1):480–487, 2018.

[26] AA Maradudin and AE Fein. Scattering of neutrons by an anharmonic crystal. *Physical Review*, 128(6):2589, 1962.

[27] José Menéndez and Manuel Cardona. Temperature dependence of the first-order raman scattering by phonons in si, ge, and α- s n: Anharmonic effects. *Physical Review B*, 29(4):2051, 1984.

[28] Terumasa Tadano and Shinji Tsuneyuki. First-principles lattice dynamics method for strongly anharmonic crystals. *Journal of the Physical Society of Japan*, 87(4):041015, 2018.

[29] Tosio Kato. *Perturbation theory for linear operators*, volume 132. Springer Science & Business Media, 2013.

[30] Stefano Baroni, Paolo Giannozzi, and Andrea Testa. Green's-function approach to linear response in solids. *Physical Review Letters*, 58(18):1861, 1987.

[31] Tianli Feng and Xiulin Ruan. Quantum mechanical prediction of four-phonon scattering rates and reduced thermal conductivity of solids. *Physical Review B*, 93(4):045202, 2016.

[32] Tianli Feng, Lucas Lindsay, and Xiulin Ruan. Four-phonon scattering significantly reduces intrinsic thermal conductivity of solids. *Physical Review B*, 96(16):161201, 2017.

[33] Tianli Feng, Xiaolong Yang, and Xiulin Ruan. Phonon anharmonic frequency shift induced by four-

phonon scattering calculated from first principles. *Journal of Applied Physics*, 124(14):145101, 2018.

[34] Michele Lazzeri, Matteo Calandra, and Francesco Mauri. Anharmonic phonon frequency shift in mgb 2. *Physical Review B*, 68(22):220509, 2003.

[35] Nicola Bonini, Michele Lazzeri, Nicola Marzari, and Francesco Mauri. Phonon anharmonicities in graphite and graphene. *Physical Review Letters*, 99(17):176802, 2007.

[36] Atsushi Togo, Laurent Chaput, and Isao Tanaka. Distributions of phonon lifetimes in brillouin zones. *Physical Review B*, 91(9):094306, 2015.

[37] Bartomeu Monserrat, ND Drummond, and RJ Needs. Anharmonic vibrational properties in periodic systems: energy, electron-phonon coupling, and stress. *Physical Review B*, 87(14):144302, 2013.

[38] Georg Kresse and Jürgen Furthmüller. Efficient iterative schemes for ab initio total-energy calculations using a plane-wave basis set. *Physical Review B*, 54(16):11169, 1996.

[39] Peter E Blöchl. Projector augmented-wave method. *Physical Review B*, 50(24):17953, 1994.

[40] John P Perdew, Kieron Burke, and Matthias Ernzerhof. Generalized gradient approximation made simple. *Physical Review Letters*, 77(18):3865, 1996.

[41] Terumasa Tadano, Yoshihiro Gohda, and Shinji Tsuneyuki. Anharmonic force constants extracted from first-principles molecular dynamics: applications to heat transfer simulations. *Journal of Physics: Condensed Matter*, 26(22):225402, 2014.

[42] Terumasa Tadano and Shinji Tsuneyuki. Self-consistent phonon calculations of lattice dynamical properties in cubic srtio 3 with first-principles anharmonic force constants. *Physical Review B*, 92(5):054301, 2015.

[43] V Zólyomi, ND Drummond, and VI Fal'Ko. Electrons and phonons in single layers of hexagonal indium chalcogenides from ab initio calculations. *Physical Review B*, 89(20):205416, 2014.

[44] Yongqing Cai, Gang Zhang, and Yong-Wei Zhang. Charge transfer and functionalization of monolayer inse by physisorption of small molecules for gas sensing. *The Journal of Physical Chemistry C*, 121(18):10182–10193, 2017.

[45] DA Broido, L Lindsay, and A Ward. Thermal conductivity of diamond under extreme pressure: a first-principles study. *Physical Review B*, 86(11):115203, 2012.

[46] Kevin D Parrish, Ankit Jain, Jason M Larkin, Wissam A Saidi, and Alan JH McGaughey. Origins of thermal conductivity changes in strained crystals. *Physical Review B*, 90(23):235201, 2014.

[47] San-Dong Guo. Biaxial strain tuned thermoelectric properties in monolayer ptse 2. *Journal of Materials Chemistry C*, 4(39):9366–9374, 2016.

[48] Liyan Zhu, Tingting Zhang, Ziming Sun, Jianhua Li, Guibin Chen, and Shengyuan A Yang. Thermal conductivity of biaxial-strained mos2: sensitive strain dependence and size-dependent reduction rate. *Nanotechnology*, 26(46):465707, 2015.

[49] Taishan Zhu and Elif Ertekin. Resolving anomalous strain effects on two-dimensional phonon flows: The cases of graphene, boron nitride, and planar superlattices. *Physical Review B*, 91(20):205429, 2015.

[50] Stefano Baroni, Stefano De Gironcoli, Andrea Dal Corso, and Paolo Giannozzi. Phonons and related crystal properties from density-functional perturbation theory. *Reviews of Modern Physics*, 73(2):515, 2001.

[51] Shobhana Narasimhan and David Vanderbilt. Anharmonic self-energies of phonons in silicon. *Physical Review B*, 43(5):4541, 1991.

[52] Lorenzo Paulatto, Ion Errea, Matteo Calandra, and Francesco Mauri. First-principles calculations of phonon frequencies, lifetimes, and spectral functions from weak to strong anharmonicity: The example of palladium hydrides. *Physical Review B*, 91(5):054304, 2015.

[53] Mois Ilia Aroyo, Juan Manuel Perez-Mato, Cesar Capillas, Eli Kroumova, Svetoslav Ivantchev, Gotzon Madariaga, Asen Kirov, and Hans Wondratschek. Bilbao crystallographic server: I. databases and crystallographic computing programs. *Zeitschrift für Kristallographie-Crystalline Materials*, 221(1):15–27, 2006.